Hindawi
Shock and Vibration
Volume 2022, Article ID 1038231, 12 pages
https://doi.org/10.1155/2022/1038231

Research Article

Application of Homogenized Load-Bearing Ring Hypothesis in Roadway Supporting

Quntao Zhang[1,2,3] **Jianwei Zheng**[4,5] **Xiaodong Sun**[2,3] **Wenzhou Li**[2,3] **Kang Yi**[1,2,3] **Yukai Fu**[2,3] **Jiulin Shi**[2,3] **Shuai Wang**[6] **Biao Liu**[7] **and Qi Wang**[8]

[1]*School of Energy, Mining Engineering, China University of Mining Technology (Beijing), Beijing 100083, China*
[2]*CCTEG Coal Mining Research Institute, Beijing 100013, China*
[3]*Coal Mining & Designing Department, Tiandi Science & Technology Co., Ltd., Beijing 100013, China*
[4]*China Coal Research Institute, Deep Mining and Rockburst Research Institute, Beijing 100013, China*
[5]*State Key Laboratory of Coal Mining and Clean Utilization, Beijing 100013, China*
[6]*China Coal Technology and Engineering Group Shenyang Research Institute, Fushun 113122, China*
[7]*Tongchuan Mining, Shaanxi Coal and Chemical Industry Group Co. Ltd., Tongchuan, Shaanxi 727101, China*
[8]*Taiyuan Institute of China Coal Technology and Engineering Group, Taiyuan 030006, China*

Correspondence should be addressed to Jianwei Zheng; zhengjanvy@163.com

Received 3 April 2022; Revised 30 April 2022; Accepted 3 May 2022; Published 24 May 2022

Academic Editor: Tao Meng

Artificial support system takes advantages of self-bearing capacity of surrounding rock mass in roadway support, which is one of the important supporting ideas in modern times. The implementation way of an artificial support system is worthy of deep investigation. In this study, an HLBR hypothesis was proposed with comprehensive consideration of mechanical properties of surrounding rock mass based on the reinforced arch theory and axial variation theory. A model of bearing structure in surrounding rock mass was constructed, and the stress state on the bearing structure was analyzed. It was believed that when the axial ratio (k) of this bearing structure is equal to the lateral stress factor (λ) (which is the optimal axial ratio), the tangential stress on the bearing boundary reaches the minimum and is in uniform distribution. At this moment, the roadway and the supporting structure can make good use of the self-carrying capacity of surrounding rock mass, which is conducive to lowering the stress distribution level of surrounding rock mass. According to prestress diffusion characteristics of bolt, some ways to achieve HLBR were proposed, which were the optimal axial ratio design, difference support and local grouting modification, and finally performance of the original support design in a belt roadway of the mining district IV of a mine in Shanxi Province. A new supporting scheme was provided according to the HLBR hypothesis. In addition, the FLAC3D strain-softening model was modified by C++, which was used to interpret the reasonability of the suggested supporting scheme. The proposed HLBR hypothesis discloses ways to use self-capacity of surrounding rock mass. This study provides a new idea for roadway sectional design and roadway support design, which are beneficial to maintaining the stability of surrounding rock mass in roadways.

1. Introduction

Stability control of surrounding rock mass in a roadway has been one of the key problems against safety recycling of underground coal resources in China. With the increase of mining depth, geological environment and stress environment where the roadway locates in become more and more complicated, accompanied by increasing difficulties in corresponding roadway support and serious threats to operation safety of underground workers [1, 2]. Based on theoretical analysis, laboratory analysis, and field studies, many scholars have investigated stability of surrounding rock mass from the perspectives of action of stress and strengthening of surrounding rock mass. The action of stress is to propose the corresponding control theories by analyzing stress that induces roadway deformation, such as the

classical circular roadway based on elastic theory [3] and stress analysis of oval roadway [4–8]. The strengthening of surrounding rock mass means increasing the bearing capacity of surrounding rock mass through artificial measures, which covers classical collapse arch theory [9, 10] and surrounding rock mass strengthening theory based on self-stability ability of surrounding rock mass as well as the collaborative action of artificial support and surrounding rock mass [11–14]. These theories solve the support problem of some roadway to some extent. Among the theories, the energy supporting theory [15] analyzes the action mechanism of support from the perspective of energy equilibrium of surrounding rock mass. The collapse arch theory [16] emphasizes the self-stability of surrounding rock mass. The hanging theory [17] belongs to the scope of the passive support mechanism of bolt. The reinforced arch theory [18], combined with arch theory and surrounding rock mass theory, can be viewed as strengthening physical mechanical properties of surrounding rock mass and forming a good bearing structure. Yang et al. believed that existing supporting technologies can be mainly divided into three types [19], including positive internal support of surrounding rock mass, passive surface support of roadway [20], and modified support [21, 22]. Gao et al. [23] analyzed the coal rock mass fractal evolution caused by mining at different depths and provided a foundation for roadway supporting. Kang et al. [24] proposed the concept of support stress field and emphasized the collaboration mechanism among supporting stress field, mining-induced stress, and primary rock stress field. They believed that the application of prestressed bolt and cable can make surrounding rock mass on roadway surface recover to three-direction stress states to some extent and increase the bearing capacity of surrounding rocks. The axial variation theory was proposed by Yu [25, 26], and the self-stabilization balance ring theory was proposed by Huang et al. [27]. The loosing ring theory [28, 29] believed that the artificial supporting object was the bulking force during the formation of loosing ring of surrounding rock mass. Zhang et al. [30] carried out a simulation analysis of four different strengthened U-shaped steel structures and found that the U-shaped steel structure with beams and longitudinal beams can offer good support to uniformly distributed loads of the roadway.

Existing roadway supporting theories and corresponding supporting methods [31–36] lay solid foundations for stability control of surrounding rock mass. With the increase of research depth, science researchers emphasize the self-bearing effect of surrounding rock mass, but relevant deep studies on ways to achieve self-bearing effect of surrounding rock mass are needed. Based on the reinforced arch and axial variation theory, this study proposed the homogenized load-bearing ring (HLBR) hypothesis with comprehensive consideration of mechanical properties of surrounding rock mass and introduced ways to achieve self-bearing capacity of surrounding rock mass. Subsequently, some optimization suggestions for the supporting design of the belt roadway of mining district IV of a mine in Shanxi Province were proposed according to the HLBR hypothesis. Moreover, the new supporting design was verified through a numerical simulation method.

2. Concept of the HLBR

The space with certain functions which is excavated in strata is called roadway (chamber). Excavation of roadway breaks the equilibrium state of the primary rock stress field within a certain range and induces redistributions of stress in surrounding rock mass, thus forming stress gradients. The roadway may develop deformation failure when the secondary stress in local positions of a roadway edge exceeds the ultimate strength of surrounding rock mass. Without external support, the surrounding rock mass is destroyed and separated from the matrix. Geometric morphology of roadway section is changed, thus changing the distribution of stress field. Roadway failure stops when the stress at surrounding rock mass boundary is lower than the ultimate strength of surrounding rock mass in the roadway. The mutual feedback process between geometrical morphology and boundary stress of roadway section is called self-stabilization (self-organized equilibrium) of surrounding rock mass in roadways. Based on abundant field observation, the final geometric morphology when surrounding rock mass reaches self-stabilization after failure can be abstracted into an "ellipse" with a certain axial ratio (the best axial ratio) or "similar ellipse." In other words, the (similar) elliptical section with the best axial ratio has good self-bearing (self-stabilization) performances under specific stress field conditions. Therefore, if the roadway is designed into an elliptical section with the best axial ratio, the stress field distribution of surrounding rock mass is optimized in favor of stability control of surrounding rock mass. Theoretically, it can develop the self-bearing (self-stability) capacity of surrounding rock mass well. However, practical design of roadway section shall integrate various influencing factors, such as construction technological level, maximum equipment size in roadway, and usage as well as service life of roadways. Geometric morphology of roadway section must be compromised to some extent, thus resulting in the abovementioned uneven stress gradients.

During roadway support, the supporting stress which is applied to surrounding rock mass artificially will be diffused in surrounding rock mass and form a load-bearing structure in the roadway. Surrounding rock mass in this load-bearing structure is in the three-direction stress states, and it can bear relatively high external loads. With consideration of the physical and mechanical properties of surrounding rock mass, this study proposed the HLBR hypothesis of surrounding rock mass in the roadway based on reinforced arch theory and axial variation theory. The load-bearing ring refers to a cyclic bearing structure in the artificial supporting system that undertakes external loads formed in surrounding rock mass. This load-bearing structure has a large bearing capacity, and its range and bearing characteristics are influenced by stress environment, roadway section, and artificial support. When the axial ratio of load-bearing ring is close to the best axial ratio of the roadway in the local geological and stress field environment, the bearing capacity of surrounding rock mass can be fully used. Under this circumstance, the load-bearing ring formed in surrounding rock mass is called an HLBR. Moreover, the goal of

reasonable support to roadway is to promote the HLBR with the optimal axial ratio in the surrounding rock mass to bear most external loads. The HLBR is composed of ultimate external bearing boundary and ultimate internal bearing boundary. The ultimate external bearing boundary refers to the maximum inscribed ellipse envelope curve that connects ends of bolts, while the ultimate internal bearing boundary refers to the minimum ellipse envelope curve, which is connected to the roadway section. The equivalent bearing section refers to the curved surface formed by the centerline of the HLBR profile. The real roadway section is called an internal section. Distributed zone of prestress bolt refers to the range in the rock mass, generated by prestress bolt. Superposed stress field of prestress bolt refers to the superimposed part between stress zone generated by different bolts. Bare roadway stabilization boundary refers to the boundary of roadway which can maintain stability without artificial supporting. The HLBR model of surrounding rock mass in the roadway is shown in Figure 1.

3. Mechanical Analysis of the HLBR

3.1. Description of Mechanical Model of the HLBR. A model of roadway surrounding rock mass was constructed based on elastic mechanics. Necessary and sufficient conditions to form the HLBR in roadway surrounding rock mass and the mechanical behaviors of this ring under external loads were analyzed. Bearing boundary conditions of surrounding rock mass were simplified. Moreover, five basic hypotheses which conform to elastic mechanics were proposed for surrounding rock mass. Stress conditions of the load-bearing ring of roadway surrounding rock mass are shown in Figure 2. In Figure 2, $2a_o$ and $2b_o$ are long axis and short axis of the external bearing boundary, while $2a_i$ and $2b_i$ are long axis and short axis of the internal bearing boundary. The elliptical load-bearing ring was simplified, and it was equivalent to the analysis of mechanical behaviors of equivalent ellipse (equivalent section) under two-way loading conditions. The intersection points between the equivalent section in Figure 2 and the X-axis are X and $X`$, whereas the intersection points between the equivalent section and the $Y$-axis are Y and Y`.

3.2. Deduction of Mechanical Model of the HLBR. Stress expression at different points of the equivalent section (equivalent ellipse) boundary, which is formed in roadway surrounding rock mass under two-way loads, was set up by using a function of complex variables [37]:

$$\begin{aligned}(\sigma_\theta)_{\xi_0} = &\left[\frac{\sinh 2\xi_0\left(1+e^{-2\xi_0}\right)}{\cosh 2\xi_0 - \cos 2\theta} - 1\right]e^{2\xi_0}P_h \\ &+\left[\frac{\sinh 2\xi_0\left(e^{-2\xi_0}-1\right)}{\cosh 2\xi_0 - \cos 2\theta} + 1\right]e^{2\xi_0}P_v,\end{aligned} \tag{1}$$

where ξ_0 is the distance from the center of equivalent ellipse to boundaries. θ is the direction angle between the research points and long axis of equivalent ellipse. $\sigma_{\theta(\zeta 0)}$ is the tangential stress on any point of boundary of equivalent ellipse. P_v is the vertical stress that the equivalent ellipse bears. P_h is the horizontal principal stress that the equivalent ellipse bears.

The auxiliary equations are shown in equations (2)–(7), where 2a is the long axis of equivalent ellipse, 2b is the short axis of equivalent ellipse, and 2c is the focal length of equivalent ellipse. Besides, there is $c^2 = a^2\text{-}b^2$:

$$\cosh\xi_0 = \frac{a}{c}, \tag{2}$$

$$\sinh\xi_0 = \frac{b}{c}, \tag{3}$$

$$\sinh 2\xi_0 = 2\cosh\xi_0 \sinh\xi_0 = \frac{2ab}{c^2} = \frac{e^{2\xi_0} - e^{-2\xi_0}}{2}, \tag{4}$$

$$\cosh 2\xi_0 = \cosh{\xi_0}^2 + \sinh{\xi_0}^2 = \frac{a^2+b^2}{c^2} = \frac{e^{2\xi_0} + e^{-2\xi_0}}{2}, \tag{5}$$

$$e^{2\xi_0} = \cosh 2\xi_0 + \sinh 2\xi_0 = \frac{(a+b)^2}{c^2} = \frac{a+b}{a-b}, \tag{6}$$

$$e^{-2\xi_0} = \cosh 2\xi_0 - \sinh 2\xi_0 = \frac{(a-b)^2}{c^2} = \frac{a-b}{a+b}. \tag{7}$$

Let $a = kb$, where k refers to the axial ratio of stress ellipse ($k > 0$ and $k \neq 1$). Let $P_h = \lambda P_v$, where λ is a lateral stress factor ($\lambda > 0$). Equation (1) can be rewritten based on equations (2)–(7), thus getting the expression (8) of equivalent ellipse boundary stress. Moreover, σ_θ can be viewed as a function of $\theta(\theta \in [0, 2\pi])$:

$$(\sigma_\theta)_{\xi_0} = \frac{2kP_v(k-\lambda)}{\left(k^2\sin^2\theta + \cos^2\right)(k-1)} + \frac{P_v(k+1)(\lambda-1)}{(k-1)}. \tag{8}$$

For (8), derivatives of θ were calculated at two sides of the equation, thus getting the expression of maximums:

$$\frac{\partial(\sigma_\theta)_{\xi_0}}{\partial\theta} = \frac{2kP_v(\lambda-k)}{(k-1)} \times \frac{\left(1-k^2\right)\sin 2\theta}{\left(k^2\sin^2\theta + \cos^2\theta\right)^2}. \tag{9}$$

It can be seen from (9) that maximums can be calculated when $\theta = 0$ and $\theta = \pi/2$. According to symmetry, the maximums can be gained when $\theta = \pi$ and $\theta = 3\pi/2$. In other words, the intersection points between stress ellipse and coordinate axis (X, $X`$, Y, and Y′) are maximum locations. Therefore, $\theta = 0$, $\theta = \pi$, $\theta = \pi/2$, and $\theta = 3\pi/2$ were brought into equation (8), thus getting stress maximums of the stress ellipse on the horizontal and vertical axes ($\sigma_{\theta(\xi 0)\,(-)}$ and $\sigma_{\theta(\xi 0)\,(\perp)}$) as follows:

$$\begin{aligned}(\sigma_\theta)_{(\xi=\xi_0)(-)} &= (2k+1-\lambda)P_v, \\ (\sigma_\theta)_{(\xi=\xi_0)(\perp)} &= \frac{2\lambda + k\lambda - k}{k}P_v.\end{aligned} \tag{10}$$

3.3. Mechanical Analysis of the HLBR. Types of tangential stress and maximum location on the equivalent ellipse under

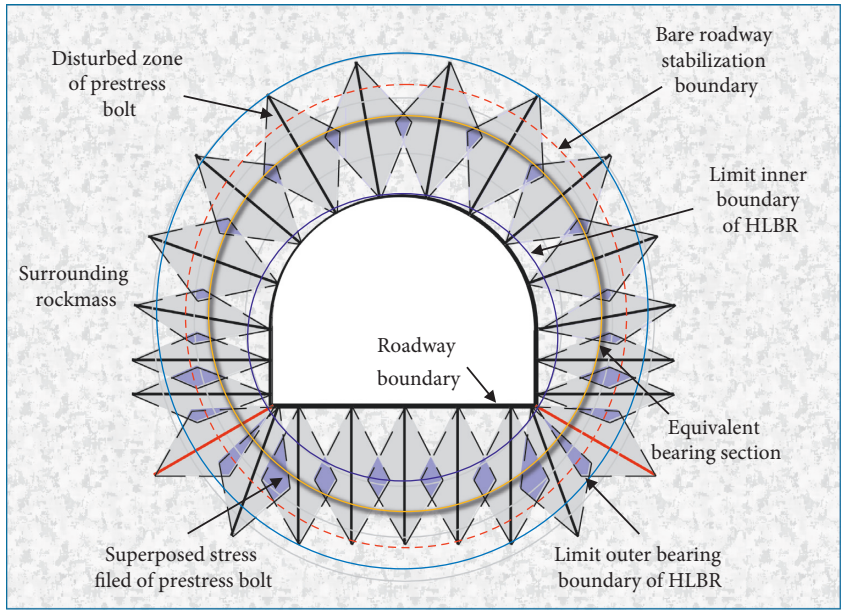

Figure 1: Model of HLBR.

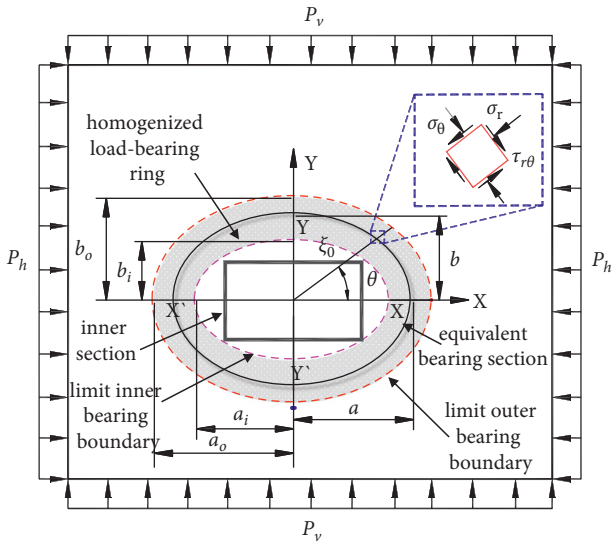

Figure 2: Mechanical model of simplified load-bearing ring in roadway surrounding rock mass.

different relationships between axial ratio of equivalent ellipse and lateral stress factor are shown in Table 1.

Based on the determined types of tangential stress and maximum locations on equivalent ellipse, tensile tress and zero stress can only be developed on X and $X`$ when $\lambda \geq 1$. Similarly, tensile stress and zero stress are developed on Y and Y′ only when $\lambda \leq 1$. The relation (qualitative trend description) between changes of lateral stress factor and changes of tangential stress factor on boundary is shown in Figure 3. The distribution characteristics of tangential stress concentration factor on the ellipse boundary with a fixed constant axial ratio under different lateral stress factors are shown in Figure 3(a). Aiming to make the rules clear, the axial ratio and lateral stress factors suppose that $k = 3$ and $\lambda = 0.2$, 0.4, 0.6, 1, 2, 3, 4, 5, 7, 8, and 10. The distribution characteristics of tangential stress concentration factor on the ellipse boundary under a fixed constant lateral factor and different axial ratios when $\lambda < 1$ are shown in Figure 3(b), in which it supposes that $\lambda = 0.5$ and $k = 0.3$, 0.4, 0.5, 0.8, 1.5, 2, 3, and 4. The distribution characteristics of tangential stress concentration factor on the ellipse boundary under a fixed constant lateral factor and different axial ratios when $\lambda > 1$ are shown in Figure 3(c), in which $\lambda = 5$ and $k = 0.9$, 1.5, 2, 3, 4, 5, 7, and 8.

Given a fixed axial ratio in Figure 3(a), surrounding rock mass on roof and floor of roadway changed from tensile failure to compressive failure with the increase of lateral stress coefficient, while the surrounding rock mass on two sides of the roadway changed from compressive failure to tensile failure. Given a fixed lateral stress factor, the failure mode of surrounding rock mass on roof and floor of roadway with the increase of axial ratio shall be determined according to specific situations. It can be seen from Figure 3(b) that surrounding rock mass on roof and floor of roadway changes from compressive failure to tensile failure, but two sides of the roadway have been bearing compressive stress, without tensile stress. With the increase of k, the compressive stress on two sides of roadway increases. It can be seen from Figure 3(c) that surrounding rock mass on two sides of roadway changes from tensile failure to compressive failure. The surrounding rock mass on the roof and floor has been under the compressive stress. Meanwhile, the compressive stress decreases with the increase of k.

Tensile strength of surrounding rock mass is far smaller than the compressive strength. Let R_t be the tensile strength of surrounding rock mass in a roadway. In this section, only longitudinal axis is analyzed. Six stress states at Y and Y` can be gained by analyzing the relationship between $\sigma_{\theta(\xi 0)\,(\perp)}$ and tensile strength of surrounding rock mass (R_t). These six stress states are strong tensile stress state (I), ultimate tensile

Table 1: Types of tangential stress and maximum location on the equivalent ellipse.

Function relationship between λ and k		X-axis		Y-axis		Position of extremum
		Type of tress in X point	Type of tress in X' point	Type of tress in Y point	Type of tress in Y′ point	
	$\lambda > 2k+1$	Tensile stress	Tensile stress	Compressive stress	Compressive stress	Y
$k < \lambda$	$\lambda = 2k+1$	0	0	Compressive stress	Compressive stress	Y
	$k < \lambda < 2k+1$	Compressive stress	Compressive stress	Compressive stress	Compressive stress	Y
$k = \lambda$	$k = \lambda$	Compressive stress	Compressive stress	Compressive stress	Compressive stress	$X = Y$
	$k/(2+k) < \lambda < k$	Compressive stress	Compressive stress	Compressive stress	Compressive stress	X
$\lambda < k$	$\lambda = k/(2+k)$	Compressive stress	Compressive stress	0	0	X
	$\lambda < k/(2+k)$	Compressive stress	Compressive stress	Tensile stress	Tensile stress	X

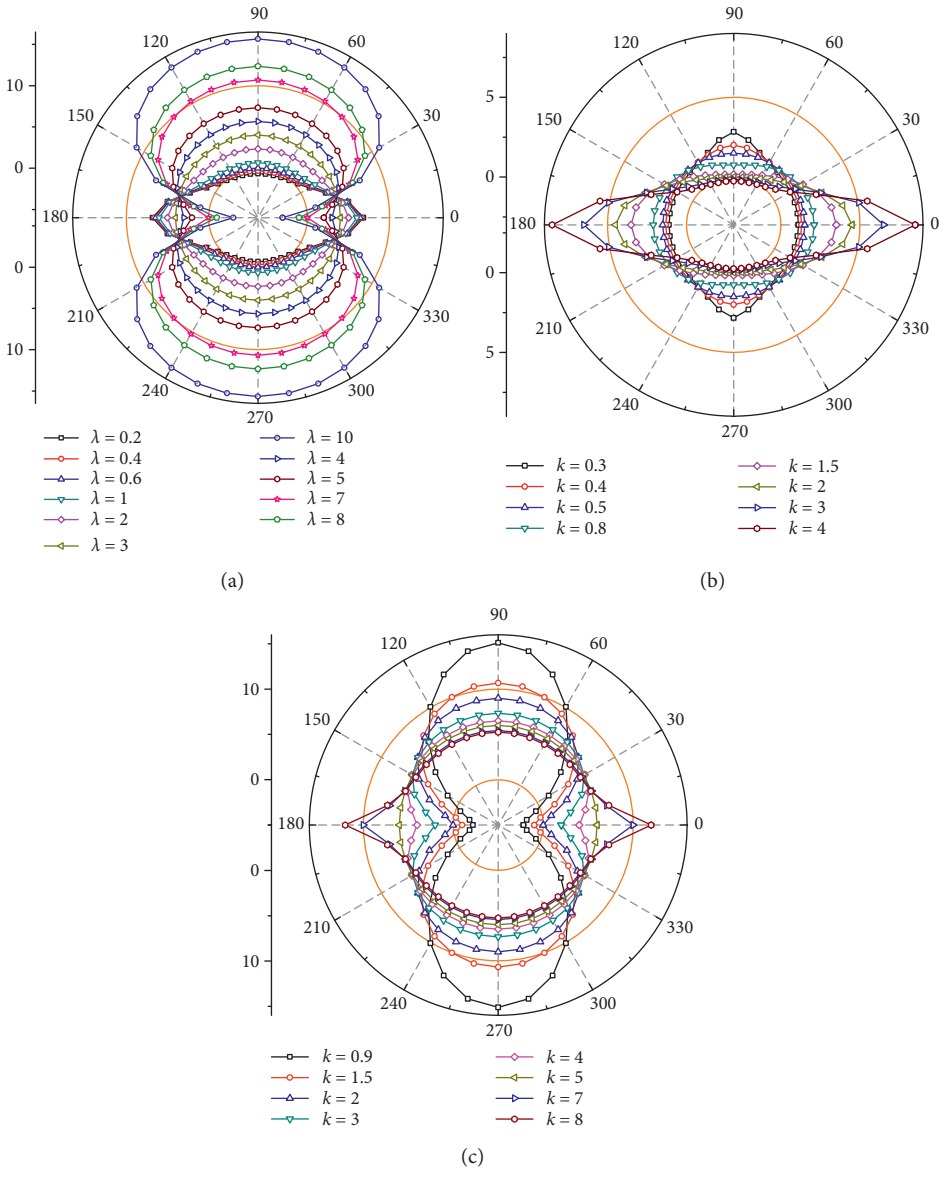

Figure 3: Distribution characteristics of tangential stress concentration factor on stress elliptic boundary under different conditions. (a) k = 3, (b) $\lambda = 0.5$, and (c) $\lambda = 5$.

stress state (*II*), weak tensile stress state (*III*), zero-stress state (*IV*), compressive stress state (*V*), and equal stress state (). When $\sigma_{\theta(\xi 0)\ (\perp)}$ at Y and Y′ is higher than the tensile strength (R_t) of surrounding rock mass ($k < 2\lambda/R_t/P_v - \lambda + 1$), Y and Y′ develop tensile failure, which can be called the strong tensile stress state (*I*). When $k = 2\lambda/R_t/P_v - \lambda + 1$, Y and Y′

are at the ultimate tensile stress state (*II*). When $\sigma_{\theta(\xi 0)\ (\perp)} > R_t$ ($k < 2\lambda/R_t/P_v - \lambda + 1$), the vertical axis end develops no tensile failure, which can be viewed as a weak tensile stress state (*III*). When $\sigma_{\theta(\xi 0)\ (\perp)} = 0$ ($k = 2\lambda/1 - \lambda$), Y and Y′ are at the zero-stress state (*IV*). When $\sigma_{\theta(\xi 0)\ (\perp)}$ is compressive stress ($k < 2\lambda/1 - \lambda$), Y and Y′ are at the compressive stress state (*V*). When $\sigma_{\theta(\xi 0)\ (\perp)}$ is a compressive stress and it is equal to $\sigma_{\theta(\xi 0)\ (-)}$ ($k = \lambda$), all points on stress ellipse boundary have equal stress and are all in a compressive stress state, which is called the equal stress state (*VI*).

The above 6 stress states of Y and Y′ were analyzed comprehensively. Stress environmental optimization of roadway surrounding rock mass shall focus on reduction of stress level and prevention of tensile stress based on strong compressive strength and poor tensile strength of surrounding rock mass. Therefore, equal stress state (*VI*) is the ideal stress state of load-bearing structure. Hence, it can be verified theoretically that stress on load-bearing ring boundary is minimum and in uniform distribution when $k = \lambda$, thus enabling us to realize the structure of HLBR.

4. Applications and Numerical Simulation Analysis of the HLBR

To elaborate the role of HLBR in supporting structure, a case study based on the supporting design of a belt roadway of the mining district IV of a mine in Shanxi Province was carried out. A numerical simulation analysis of this belt roadway was performed by FLAC3D, and the design scheme of the primary roadway supporting structure to surrounding rock mass was evaluated. A new supporting design scheme was proposed based on the HLBR hypothesis. Its performance was compared with that of the primary support design.

4.1. Model Background and Primary Support Design. The advancing section in the study area was 5.30 m wide and 3.55 m high. Stability of roadway surrounding rock mass was maintained by a compound supporting scheme of "bolt + cable + metal mesh + steel ladder beam." The row space of bolts on roof (MSGLW, 335/22 × 2400) is 800 mm × 800 mm, and the row space of bolts on two sides (MSGLW, 335/22 × 2400) is 1000 mm × 800 mm. Cable (SKP, 18.9 × 8300) was in three-flower distribution, and metal mesh used the graticules (50 mm × 50 mm) made of Φ10 iron wires. The steel ladder beam (Φ14 mm rebar) was 60 mm wide, and it was covered on the roof and two sides of the roadway. However, no prestress was applied to the bolt and cable in the supporting design. Instead, they were installed by end anchoring mode. Prestress on the bolt and cable was measured 5–10 kN and 20–30 kN, respectively. Low-strength ordinary supporting plate was applied to the bolt and cable.

4.2. Research on Roadway Geostress. A geostress measurement system was installed in the study area [38]. Measuring positions and measuring results are shown in Figure 4. According to measurement results, the maximum and minimum horizontal principal stress (σ_m and σ_l) are 9.04 MPa and 5.22 MPa, and the vertical stress (σ_v) is 8.40 MPa. Besides, the included angle between the maximum horizontal principal stress and belt roadway in mining district IV is NE20°. The coordinate transformation is shown in equations (11) and (12) [37], where σ_m is the maximum horizontal principal stress under the old coordinate system; σ_l is the minimum principal stress under the old coordinate system; σ_{ml} is the tangential stress under the old coordinate system, and there is $\sigma_{ml} = 0$; σ_x is the maximum horizontal principal stress under the new coordinate system; σ_y is the minimum principal stress under the new coordinate system; σ_y is the minimum principal stress under the new coordinate system; and θ is the deflection angle of the coordinate system. Measurement results of geostress were brought into equations (11) and (12), and stresses on two sides of the roadway were gained: $\sigma_x = 8.59$ Mpa and $\sigma_y = 5.67$ MPa. Therefore, the lateral stress factor in the roadway was $\lambda = \sigma_x/\sigma_v = 1.02$ and $k = 1.49$:

$$(\sigma_x) = \frac{1}{2}(\sigma_m + \sigma_l) + \frac{1}{2}(\sigma_m - \sigma_l)\cos 2\theta + \sigma_{ml} \sin 2\theta, \quad (11)$$

$$(\sigma_y) = \frac{1}{2}(\sigma_m + \sigma_l) - \frac{1}{2}(\sigma_m - \sigma_l)\cos 2\theta - \sigma_{ml} \sin 2\theta. \quad (12)$$

The primary support design in the study area applied the low-level prestress on bolts and cable. The primary support design was analyzed based on the HLBR hypothesis. It found that the primary support design failed to form effective positive support to load-bearing structure in surrounding rock mass, and it was only passive support. Hence, the axial ratio of bearing structure in the study area is equal to the axial ratio in the primary sectional design ($k = 1.49$) of the roadway. Moreover, the axial ratio of final self-stabilization boundaries was $k = \lambda = 1.02$ under the influences of stress redistribution. Therefore, depth of the plastic region on roof and floor during the self-stabilization of belt roadway was higher than the development depth of the plastic region on two sides of the roadway.

4.3. Optical Borehole Observation in Roadway Surrounding Rock Mass. Optical borehole observation was implemented in the belt roadway of mining district IV. Measurement results are shown in Figure 5. According to analysis, they were developed with fractured sandy mudstone within 0–1.3 m of roadway roof, medium sandstone within 1.3–4.5 m of roadway, fractures within 1.3–1.5 m of roadway, and sandy mudstone with high integrity within 4.5–7.0 m of roadway. Coal fractures since 0–0.7 m of roadway surface on sides of roadway are loose. Roadway deformation was analyzed by considering that rock mass is a homogeneous elastic material. According to the symmetric principle, failure depths of roadway roof and floor were 1.5 m, and the failure depth on two sides was 0.7 m after the roadway was drilled. The real axial ratio of roadway after the development of plastic region in the surrounding rock mass was $k_n = (2.65 + 0.7)/(1.75 + 1.5) = 1.03$, indicating a certain degree of self-stabilization of

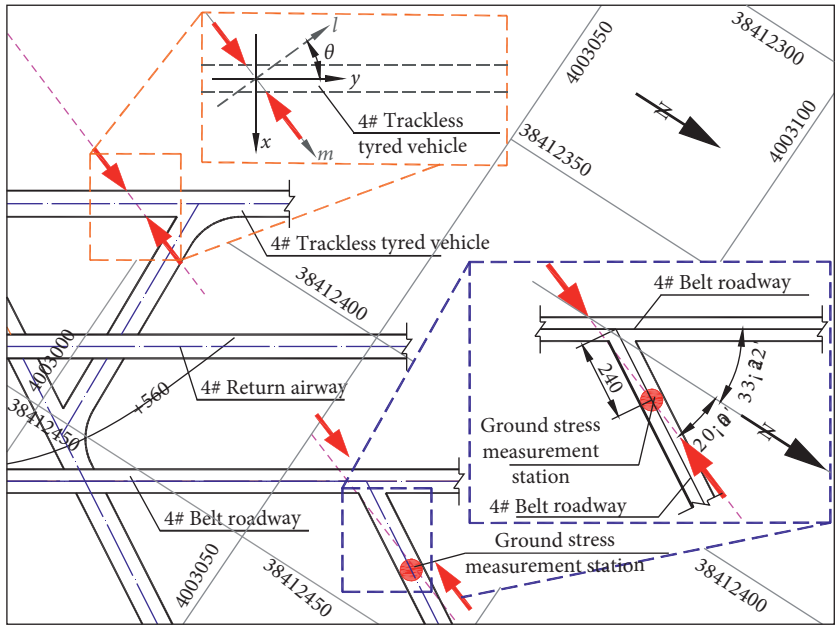

Figure 4: Measurement location and maximum horizontal stress direction of geostress in the study area.

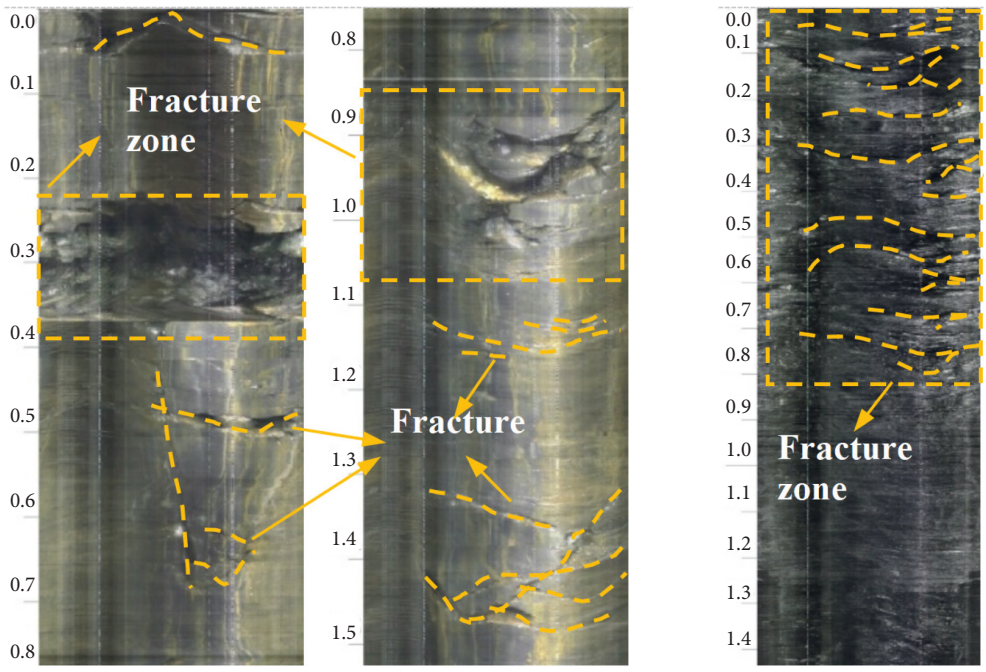

(a) Roof (b) Coal wall

Figure 5: Borehole optical observation in roof and coal seam side.

roadway under loads. The stress distribution on roadway surrounding rock mass was optimized, during which the artificial supporting system developed limited effect. The actual deformation features of the roadway basically conform to the above theoretical analysis.

4.4. Simulation on Stress Evolution of the HLBR. A numerical simulation analysis of the study area was carried out by using FLAC3D. Width, axial length, and vertical height of the model were set at 50 m, 30 m, and 47 m, respectively. The roof strata within 23 m above the coal seam were simulated, and the floor 20 m below the coal seam was rock strata. The simulation model is shown in Figure 6. The distance from the boundaries of the model to the excavation boundary exceeds 5 times of the maximum radius of the roadway. Lithological and physical mechanical parameters of rock mass on roof and floor of the roadway are shown in Table 2. The model set boundary conditions and initial conditions based on geostress test results. According to strain-softening

model analysis of coal seam and rock mass, linear approximation was implemented according to [39] in the process of strain softening. In other words, the internal frictional angle is constant in the strain-softening process. Among strength parameters, only cohesion degenerates with the increase of plastic shearing strain since softening variable has different definitions; the calculation formula of softening variable in the FLAC3D strain-softening model was modified by *C*++ and recompiled again, which is shown in equations (12) and (13) [39]:

$$c = c_0\left(1.001 - \frac{\tan h(100\eta)}{\tan h(10)}\right)^a, \qquad \eta = \gamma^p = \varepsilon_1^p - \varepsilon_3^p, \tag{13}$$

where c is the cohesion, c_0 is the initial cohesion, and a is the fitting parameter which ranges between 0.29 and 0.34 for sedimentary rocks. In this study, the mean value is 0.315. η is the softening variable, and γ^p is the plastic shearing strain. ε_1^p and ε_3^p are maximum and minimum plastic principal strains, respectively.

Simulation results of roadway surrounding rock mass under different supporting systems are shown in Figure 7. Without supporting system, the load-bearing structure formed by sectional shape of roadway surrounding rock mass is shown in Figure 7(a). The load-bearing structure of roadway surrounding rock mass in the roadway surrounding rock mass is shown in Figure 7(b). According to the comparison between Figure 7(a) and Figure 7(b), the primary supporting design fails to promote changes in load-bearing structural morphology of surrounding rock mass effectively due to the low prestress. According to different supporting philosophy in implementation of HLBR, the roadway support can be designed by combining sectional design and surrounding geostress distribution in the study area. Specifically, the length and prestress level of bolt on roof and floor are higher than those on two sides. Length of cable on roof can be lowered appropriately, but large prestress shall be applied on it. Moreover, a certain length of high-prestress cable shall be installed at the end corners of roadway. The suggested supporting scheme in Figure 7(c) is set as follows: length of bolt on roof and floor = 3.0 m, designed prestress level = 70 kN, and row space = 800 mm × 800 mm; length of cable = 6.4 m, prestress level = 300 kN, and three-flower distribution; length of cable at the end corner = 4.4 m and prestress level = 200 kN; length of bolt on two sides of roadway is adjusted to 2.0 m and the prestress level is designed 20 kN, accompanied by a row space of 800 mm × 800 mm. The load-bearing structure formed by the suggested supporting scheme in roadway surrounding rock mass is shown in Figure 7(c). According to the analysis, the suggested supporting scheme changes the geometric morphology of bearing structure effective in the roadway surrounding rock mass and promotes the formation of a homogenized load-bearing structure in the roadway surrounding rock mass. Displacement changes of roadway under no supporting scheme, primary supporting design, and the suggested supporting scheme are shown in Figures 8(a), 8(b), and 8(c). It can be seen from the comparison of Figures 8(a), 8(b), and 8(c) that the roadway displacement under the suggested supporting scheme is the minimum, indicating that the load-bearing structure under the suggested supporting scheme can offer strong supports to the roadway surrounding rock mass and thereby lower displacement of roadway.

4.5. Implementation Ways of the HLBR. The HLBR hypothesis is formed by evolutionary characteristics of collapse boundaries at natural equilibrium of surrounding rock mass based on the reinforced arch theory. When the axial ratio of load-bearing ring formed by the artificial supporting system in the roadway surrounding rock mass is equal to the optimal axial ratio of the roadway under local geology and stress conditions, the self-bearing (self-stabilization) ability of roadway surrounding rock mass can be used well in theory. As a result, stress field distribution of roadway surrounding rock mass is optimized to be in favor of stability control. Based on the above studies and other scholars' description of prestress diffusion of bolt, this study believed that the HLBR can be achieved by the following three ways, including optical axial ratio design, difference support, and local grouting modification.

4.6. Optimal Axial Ratio Design. Based on the above analysis of stress states at Y and Y′, all boundaries of roadway undertake relatively small compressive stresses, and these stress values are equal. The lateral stress factor (λ) of the region where roadway locates in is used as an index to determine the geometric morphology and size of roadway section. With consideration to practical demands of field investigation, decisions on geometric morphology and axial ratio of internal section shall be made. During the design of roadway sectional dimension under the premise of roadway functions, attention shall be paid to try to use the axial ratio (k) of the internal ellipse as the lateral stress factor on roadway surrounding rock mass (λ) but avoid the roadway sectional design in which the principal stress direction on roadway surrounding rock mass is perpendicular with long axis of the roadway. This design can make full use of self-bearing capacity of surrounding rock mass and promote roadway surrounding rock mass maintaining a relatively small stress state.

4.7. Difference Support. The axial ratio of load-bearing ring can be equal to the lateral stress factor through the bolt (cable) arrangement in different support, thus constructing an HLBR structure in roadway surrounding rock mass. Difference support is to install bolts (cables) of different lengths, different prestress levels, and row spaces (roof, floor, and two sides) on roadway surrounding rock mass to form an HLBR with the optimal axial ratio:

(1) When $k < \lambda$, the stress condition can be divided into three types, namely, $k < 1 > \lambda$, $1 < k < \lambda$, and $k < \lambda < 1$. It can be seen from equations (10) and (11) that Y and Y` have been bearing compressive stresses, whereas X and X' were easy to have tensile stresses. Therefore, load-bearing structure on two sides of

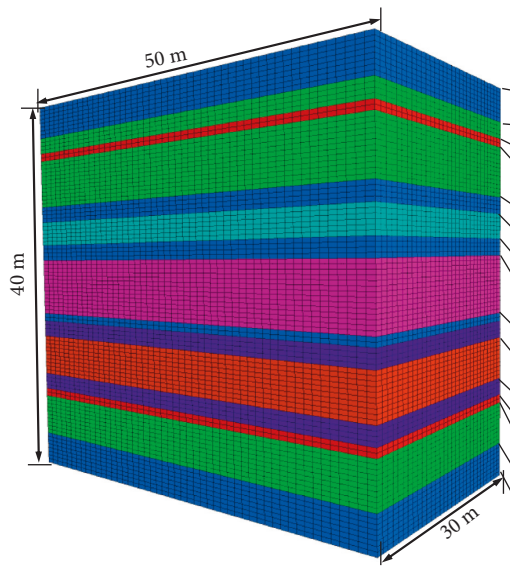

Lithology	Thickness (m)
Sandy mudstone	2.8
Fine sandstone	2.6
Mudstone	1.2
Medium sandstone	4.4
Siltite	3.9
Mudstone	3.2
Siltite	2.3
Medium sandstone	10.6
Sandy mudstone	5.94
Coal	7.52
Sandy mudstone	1.1
Fine sandstone	1.8
Siltite	4.74
Fine sandstone	2.0

Figure 6: Simulation model.

Table 2: Physicomechanical performance of coal seams and their surrounding rock mass.

Lithology	Bulk modulus (GPa)	Shear modulus (GPa)	Initial cohesion (MPa)	Internal friction angle (°)	Dilation angle (°)
Fine-grained sandstone	5.63	3.15	6.01	27.9	10.3
Mudstone	2.95	1.62	2.18	27.3	12.3
Medium sandstone	7.85	4.56	8.53	29.8	9.7
Coal	1.45	0.76	1.86	37	13.1
Siltstone	4.65	3.36	5.97	23.2	8.2
Sandy mudstone	5.85	3.11	4.33	26.7	15.6

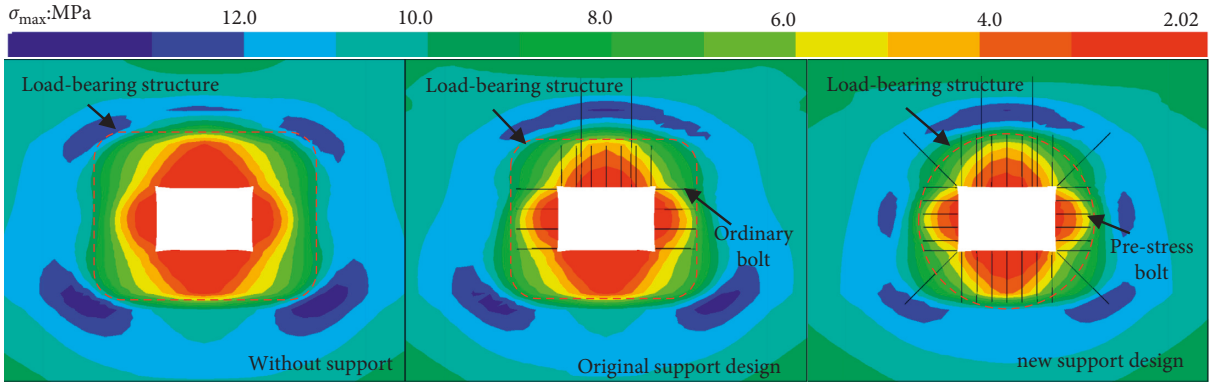

(a) (b) (c)

Figure 7: Load-bearing structure and tangential stress distribution of roadway surrounding rock mass under different conditions.

roadway surrounding rock mass was constructed by increasing prestress level and length of bolts on two sides as well as decreasing the row space. The detailed length, prestress level, and row space of bolts shall be decided according to specific conditions. When $k > \lambda$, the stress condition also can be divided into three types, namely, $k > \lambda > 1$, $k > 1 < \lambda$, and $1 < k > \lambda$. Similarly, it can be seen from equations (10) and (11) that Y and Y′ are easy to develop tensile stress. In the same way, a load-bearing structure on roof and floor of roadway surrounding rock mass also can be constructed by increasing prestress level on roof and floor, length of bolts, and row space.

(2) It is easy to have high-stress concentration on the corner of the section center in the roadway. Supplementary support with high-prestress bolts (cables) at the corner is needed. On the one hand, the bolts (cable) at the end corner can control the corner deformation of the roadway. On the other hand, they

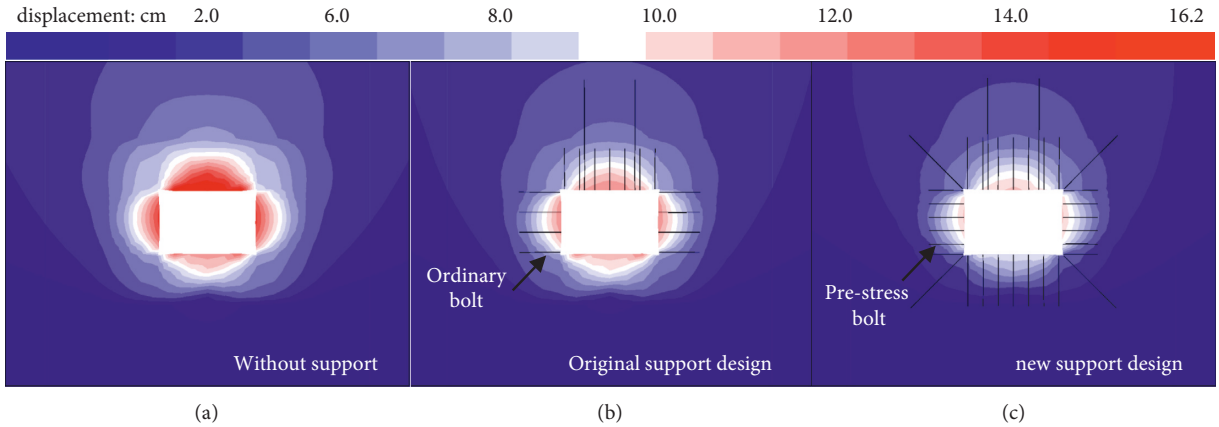

Figure 8: Displacement of roadway surrounding rock mass under different conditions.

can maintain the correlation between roof and floor and stress diffusion range at two sides, forming a complete load-bearing structure. Axial ratio (k) of equivalent section can be adjusted by controlling the length and row space of bolts (cables) on the roadway section. Consequently, the equivalent section presents a state of equal stresses ($k = \lambda$).

(3) A full sectional support is needed due to the strong stress and unique geological conditions of the roadway in order to assure a closed stress diffusion range of roof-sides-floor of roadway. Such closed complete sectional support is in favor of forming a complete HLBR structure in roadway surrounding rock mass and preventing large roadway deformation due to inadequate bearing capacity and stress releasing in local regions. If support to floor is simplified, it is inevitable to have certain heaving on floor. When the roadway lies in good geological conditions and heaving floor can meet demands for safety production, the acceptable simple support to the floor can be designed from perspectives of economy and construction speed.

4.8. Local Grouting Modification. Priestess field of bolt is formed by the nut torque which is applied at end of bolts in roadway surrounding rock mass. Many scholars have carried out abundant theoretical and experimental studies on the range and morphology of prestress field in the roadway surrounding rock mass [40–44]. Results demonstrated that the integrity degree of roadway surrounding rock mass (fracture development degree) and its mechanical properties determine the formation of prestress field. When there is a development of low-strength fractures in roadway surrounding rock mass, primary support and grouting reinforcement in local areas shall be installed in time during the tunnel advancing, followed by application of prestress on surrounding rock mass.

Grouting measures can fill in primary and secondary fractures in surrounding rock mass, thus increasing the integrity and overall strength of roadway surrounding rock mass and realizing the goal of physical modification to surrounding rock mass. On the one hand, increasing the integrity and strength of roadway surrounding rock mass promotes the formation of a prestress field by single bolt in surrounding rock mass and a prestress overlapping field by multiple bolts, thus making surrounding mass in the prestress overlapping field bear three-direction loads and achieving a higher load-bearing capacity. On the other hand, it can lower loss of prestress on bolt, so that the anchor road can maintain a certain diffusion range of prestress field for a long period. This is beneficial to the long-term bearing capacity of roadway surrounding rock mass. Local grouting modification in roadway surrounding rock mass can promote the formation and long-term stability of prestress field caused by bolts. Applying prestress again to the surrounding rock mass after grouting modification is a compensation for the lost prestress of bolts due to surrounding rock mass deformation. It not only assures the formation of internal prestress diffusion range of bolts in surrounding rock mass but also is conducive to the formation and effective maintaining of the HLBR in roadway surrounding rock mass.

5. Discussion

Three ways, including optical axial ratio design, difference support, and local grouting modification, are proposed to reach the goal of roadway supported by the HLBR hypothesis. Firstly, optical axial ratio design refers to the design progress of roadway; the idea of optical axial ratio design should be concerned when designing the roadway section. Difference support means that ellipse-shaped superposed stress field could be achieved by different support parameter. Local grouting modification is the common method to strengthen the roadway surrounding rock mass. It is demonstrated that a good use of self-carrying capacity of surrounding rock mass can be achieved by the three ways mentioned above, which is conducive to lowering the stress distribution level of surrounding rock mass and maintaining the stability of roadway.

6. Conclusions

In addition, the conclusions should be simplified.

(1) With comprehensive consideration of mechanical properties of roadway surrounding rock mass, this

study proposes an HLBR hypothesis based on reinforced arch theory and axial variation theory. This hypothesis points out that the axial ratio (k) of load-bearing ring formed by an artificial supporting system in roadway surrounding rock mass is equal to or similar to the ratio between horizontal principal stress and vertical principal stress (λ, which is the optimal axial ratio) in the roadway. Stress on this load-bearing ring is the minimum and uniform distribution, thus forming an HLBR. The roadway and supporting structure can make full use of self-bearing capacity of roadway surrounding rock mass, which is beneficial to stress distribution of roadway surrounding rock mass.

(2) Given a fixed axial ratio, surrounding rock mass on roof and floor changes from tensile failure to compressive failure, while the surrounding rock mass on two sides changes from compressive failure to tensile failure with the increase of lateral stress factor. When the lateral stress factor is fixed, there are two situations with the increase of the axial ratio of the roadway.

   (1) When $\lambda < 1$, surrounding rock mass on roof and floor changes from compressive failure to tensile failure, but no tensile stress is developed on surrounding rock mass on two sides of the roadway. Compressive stress on two sides of the roadway increases with the increase of k.
   (2) When $\lambda > 1$, the surrounding rock mass on two sides of the roadway changes from tensile failure to compressive failure, and the surrounding rock mass on roof and floor has been bearing compressive stress. Compressive stress on roof and floor decreases with the increase of k.

(3) There are three ways to form an HLBR, which are optimal axial ratio design, difference support, and local grouting modification. The optimal axial ratio design means that the axial ratio of internal ellipse of roadway section shall try to be equal to lateral stress coefficient in the roadway. Difference support promotes the formation of HLBR in roadway surrounding rock mass by designing different lengths, prestress level, and row space (roof, floor, and two sides) of bolt. Local grouting modification is to make physical modification to surrounding rock mass by grouting measures, and prestress is applied again to assure the formation of stress diffusion range in surrounding rock mass. This is beneficial to the formation of an HLBR.

Data Availability

The data used to support the findings of this study are included within the article.

Conflicts of Interest

The authors declare that they have no conflicts of interest.

Acknowledgments

This research was funded by the National Natural Science Foundation of China (Grant no. 52104091), Tiandi Science and Technology Co., Ltd. Science and Technology Innovation Venture Capital Special Project, (Grant nos. 2020-2-ZD001, 2019-TD-ZD008, KCYJY-2021-ZD-02, and KJ-2021-KCZD-02), and Fundamental Research Program of Shanxi Province (Grant no. 20210302124488).

References

[1] G. Li, Y. Hu, S.-m. Tian, M. weibin, and H.-l. Huang, "Analysis of deformation control mechanism of prestressed anchor on jointed soft rock in large cross-section tunnel," *Bulletin of Engineering Geology and the Environment*, vol. 80, no. 12, pp. 9089–9103, 2021.

[2] A. Batugin, Z. Wang, Z. Su, and S. S. Sidikovna, "Combined support mechanism of rock bolts and anchor cables for adjacent roadways in the external staggered split-level panel layout," *International Journal of Coal Science & Technology*, vol. 8, no. 4, pp. 659–673, 2021.

[3] A. Fahimifar and A. R. Hedayat, "Elasto-plastic analysis in conventional tunnelling excavation," *Proceedings of the Institution of Civil Engineers - Geotechnical Engineering*, vol. 163, no. 1, pp. 37–45, 2010.

[4] Q. Wang, M. He, S. Li et al., "Comparative study of model tests on automatically formed roadway and gob-side entry driving in deep coal mines," *International Journal of Mining Science and Technology*, vol. 31, no. 4, pp. 591–601, 2021.

[5] B. H. G. Brady and E. T. Brown, *Rock Mechanics for Underground Mining*, Springer, London, UK, 2006.

[6] W. J. Gale and R. L. Blackwood, "Stress distributions and rock failure around coal mine roadways," *International Journal of Rock Mechanics and Mining Sciences & Geomechanics Abstracts*, Pergamon, vol. 24, no. 3, , pp. 165–173, Australia, 1987.

[7] P. Zhang, D. F. Zhang, Y. Yang et al., "A case study on intergrated modeling of spatial information of a complex geological body," *Lithosphere*, vol. 2022, no. 10, Article ID 2918401, 2022.

[8] Y. Wang, H. N. Yang, J. Q. Han, and C. Zhu, "Effect of rock bridge length on fracture and damage modelling in granite containing hole and fissures under cyclic uniaxial increasing-amplitude decreasing-frequency (CUIADF) loads," *International Journal of Fatigue*, vol. 158, Article ID 106741, 2022.

[9] R. L. Handy, "The arch in soil arching," *Journal of Geotechnical Engineering*, vol. 111, no. 3, pp. 302–318, 1985.

[10] K. Terzaghi, *Theoretical Soil Mechanics*, John Wiley & Sons, New York, USA, 1943.

[11] M. G. Qian, P. W. Shi, and J. L. Xu, *Mining Pressure and Strata Control*, China University of Mining and Technology Press, Xuzhou, China, 2010.

[12] C. C. Li, "Rock support design based on the concept of pressure arch," *International Journal of Rock Mechanics and Mining Sciences*, vol. 43, no. 7, pp. 1083–1090, 2006.

[13] D. Chen, H. Chen, W. Zhang, J. Lou, and B. Shan, "An analytical solution of equivalent elastic modulus considering confining stress and its variables sensitivity analysis for fractured rock masses," *Journal of Rock Mechanics and Geotechnical Engineering*, vol. 14, no. 3, pp. 825–836, 2021.

[14] C. Hou, N. Zhang, X. Li, and P. Gou, "Study on the strength enhancement theory of surrounding rock by bolting," *Modern Tunneling Science and Technology*, vol. 1, pp. 195–197, 2017.

[15] C. Wang, L. Liu, D. Elmo et al., "Improved energy balance theory applied to roadway support design in deep mining," *Journal of Geophysics and Engineering*, vol. 15, no. 4, pp. 1588–1601, 2018.

[16] B. A. Poulsen, "Coal pillar load calculation by pressure arch theory and near field extraction ratio," *International Journal of Rock Mechanics and Mining Sciences*, vol. 47, no. 7, pp. 1158–1165, 2010.

[17] Y. Zhang, X. Wang, L. Zhao, J. Liu, N. Wang, and Y. Ding, "Mechanical performance study of the retractable pier column after stiffening," *International Journal of Coal Science & Technology*, vol. 7, no. 4, pp. 725–739, 2020.

[18] J. W. Zheng, W. J. Ju, and Z. Zhang, "Equivalent section supporting theory and its applications," *Journal of China Coal Society*, vol. 45, no. 3, pp. 1036–1043, 2020.

[19] S. Q. Yang, M. Chen, H. W. Jing, K. F. Chen, and B. Meng, "A case study on large deformation failure mechanism of deep soft rock roadway in Xin'An coal mine," *China." Engineering Geology*, vol. 217, pp. 89–101, 2016.

[20] Y.-Y. Jiao, L. Song, X.-Z. Wang, and A. Coffi Adoko, "Improvement of the U-shaped steel sets for supporting the roadways in loose thick coal seam," *International Journal of Rock Mechanics and Mining Sciences*, vol. 60, pp. 19–25, 2013.

[21] J. H. Chen, H. B. Zhao, F. L. He, J. Zhang, and K. Tao, "Studying the performance of fully encapsulated rock bolts with modified structural elements," *Int J Coal Sci Technol*, vol. 8, no. 1, pp. 64–76, 2021.

[22] B. Nikbakhtan and M. Osanloo, "Effect of grout pressure and grout flow on soil physical and mechanical properties in jet grouting operations," *International Journal of Rock Mechanics and Mining Sciences*, vol. 46, no. 3, pp. 498–505, 2009.

[23] M. Z. Gao, J. Xie, J. Guo, Lu Yiqiang, He Zhiqiang, and Li Cong, "Fractal evolution and connectivity characteristics of mining-induced crack networks in coal masses at different depths," *Geomechanics and Geophysics for Geo-Energy and Geo-Resources*, vol. 7, no. 1, 2021.

[24] H. P. Kang, G. F. Wang, P. F. Jiang et al., "Conception for strata control and intelligent mining technology in deep coal mines with depth more than 1 000 m," *Journal of China Coal Society*, vol. 43, pp. 1789–1800, 2018.

[25] X. F. Yu and D. Qiao, "Theory of axial variation and three rules of axial ratio for stabilizing country rock," *Nonferrous Metals*, vol. 8, pp. 21–25, 1981.

[26] X. F. Yu, "A theory on ground pressure: axial variation," *Nonferrous Metals*, vol. 16, pp. 9–18, 1959.

[27] Q. X. Huang and Z. Q. Shi, "Theory of equilibrium circle of roadway in three soft coal seam," *Journal of Xi'an University of Science and Technology*, vol. 36, pp. 331–335, 2016.

[28] W. Zhang, X.-b. Li, and F.-q. Gong, "Stability classification model of mine-lane surrounding rock based on distance discriminant analysis method," *Journal of Central South University of Technology*, vol. 15, no. 1, pp. 117–120, 2008.

[29] Y. Li, X. Tang, S. Yang, and J. Chen, "Evolution of the broken rock zone in the mixed ground tunnel based on the DSCM," *Tunnelling and Underground Space Technology*, vol. 84, pp. 248–258, 2019.

[30] S. Zhang, J. Li, and J. Ma, "Roadway supporting technology applied to three soft coal seam at yanlong mining area in China," *Thermal Science*, vol. 23, no. Suppl. 3, pp. 887–895, 2019.

[31] Z. Ding, J. Jia, and R. Feng, "Effect of the vertical stress on CO 2 flow behavior and permeability variation in coalbed methane reservoirs," *Energy Science & Engineering*, vol. 7, no. 5, pp. 1937–1947, 2019.

[32] X. Li, Q. Li, Y. J. Hu et al., "Study on three-dimensional dynamic stability of open-pit high slope under blasting vibration," *Lithosphere*, vol. 2021, no. 4, p. 6426550, 2022.

[33] Z. Dou, S. Tang, X. Zhang et al., "Influence of shear displacement on fluid flow and solute transport in a 3D rough fracture," *Lithosphere*, vol. 2021, no. Special 4, p. 1569736, 2021.

[34] Z.-j. Wu, Z.-y. Wang, L.-f. Fan, L. Weng, and Q.-s. Liu, "Micro-failure process and failure mechanism of brittle rock under uniaxial compression using continuous real-time wave velocity measurement," *Journal of Central South University*, vol. 28, no. 2, pp. 556–571, 2021.

[35] Q. Yin, J. Y. Wu, Z. Jiang et al., "Investigating the effect of water quenching cycles on mechanical behaviors for granites after conventional triaxial compression," *Geomechanics and Geophysics for Geo-Energy and Geo-Resources*, vol. 8, no. 2, 2022.

[36] C. Zhu, M. Karakus, M. He et al., "Volumetric deformation and damage evolution of Tibet interbedded skarn under multistage constant-amplitude-cyclic loading," *International Journal of Rock Mechanics and Mining Sciences*, vol. 152, p. 105066, 2022.

[37] Z. Y. Chen, *Mechanical Analysis of Analytical Method in Surrounding Rockmass*, Coal Industry Press, Beijing, China, 1994.

[38] H. Kang, X. Zhang, L. Si, Y. Wu, and F. Gao, "In-situ stress measurements and stress distribution characteristics in underground coal mines in China," *Engineering Geology*, vol. 116, no. 3-4, pp. 333–345, 2010.

[39] O. Pourhosseini and M. Shabanimashcool, "Development of an elasto-plastic constitutive model for intact rocks," *International Journal of Rock Mechanics and Mining Sciences*, vol. 66, pp. 1–12, 2014.

[40] E. Hoek, r P. K. Kaise, and W. F. Bawden, *Support of Underground Excavation in Hard Rock*, A A Balkema Publishers, Rotterdam, Netherlands, 1995.

[41] T. A. Lang, "Theory and practice of rock bolting," *Trans AIME*, vol. 220, pp. 333–348, 1961.

[42] H. Yu, H. Jia, S. Liu, Z. Liu, and B. Li, "Macro and micro grouting process and the influence mechanism of cracks in soft coal seam," *International Journal of Coal Science & Technology*, vol. 8, no. 5, pp. 969–982, 2021.

[43] C. Chunlin Li, "A new energy-absorbing bolt for rock support in high stress rock masses," *International Journal of Rock Mechanics and Mining Sciences*, vol. 47, no. 3, pp. 396–404, 2010.

[44] W. Lu, Q. Wang, B. Jiang et al., "Comparative study on bearing mechanism and design parameters of confined concrete arch joints in deep soft rock roadway," *International Journal of Coal Science & Technology*, vol. 6, no. 4, pp. 493–504, 2019.